Miner Deposita (2009) 44:849–866
DOI 10.1007/s00126-009-0252-4

ARTICLE

The El Teniente porphyry Cu–Mo deposit from a hydrothermal rutile perspective

Osvaldo M. Rabbia · Laura B. Hernández · David H. French · Robert W. King · John C. Ayers

Received: 31 January 2009 / Accepted: 8 July 2009 / Published online: 5 August 2009

Abstract Mineralogical, textural, and chemical analyses (EPMA and PIXE) of hydrothermal rutile in the El Teniente porphyry Cu–Mo deposit help to better constrain ore formation processes. Rutile formed from igneous Ti-rich phases (sphene, biotite, Ti-magnetite, and ilmenite) by re-equilibration and/or breakdown under hydrothermal conditions at temperatures ranging between 400°C and 700°C. Most rutile nucleate and grow at the original textural position of its Ti-rich igneous parent mineral phase. The distribution of Mo content in rutile indicates that low-temperature (~400–550°C), Mo-poor rutile (5.4±1.1 ppm) is dominantly in the Mo-rich mafic wallrocks (high-grade ore), while high-temperature (~550-700°C), Mo-rich rutile (186±20 ppm) is found in the Mo-poor felsic porphyries (low-grade ore). Rutile from late dacite ring dikes is a notable exception to this distribution pattern. The Sb content in rutile from the high-temperature potassic core of the deposit to its low-temperature propylitic fringe remains relatively constant (35±3 ppm). Temperature and Mo content of the hydrothermal fluids in addition to Mo/Ti ratio, modal abundance and stability of Ti-rich parental phases are key factors constraining Mo content and provenance in high-temperature (≥550°C) rutile. The initial Mo content of parent mineral phases is controlled by melt composition and oxygen fugacity as well as timing and efficiency of fluid–melt separation. Enhanced reduction of SO_2-rich fluids and sulfide deposition in the Fe-rich mafic wallrocks influences the low-temperature (≤550°C) rutile chemistry. The data are consistent with a model of fluid circulation of hot (>550°C), oxidized ($fO_2 \geq$NNO+1.3), SO_2-rich and Mo-bearing fluids, likely exsolved from deeper crystallizing parts of the porphyry system and fluxed through the upper dacite porphyries and related structures, with metal deposition dominantly in the Fe-rich mafic wallrocks.

Keywords Rutile · El Teniente · Porphyry copper deposit · Molybdenum · Chile

Editorial handling: B. Lehmann

Electronic supplementary material The online version of this article (doi:10.1007/s00126-009-0252-4) contains supplementary material, which is available to authorized users.

O. M. Rabbia (✉) · L. B. Hernández
Instituto GEA, Casilla 160-C, Universidad de Concepción,
Concepción 3, Chile
e-mail: rabbia@udec.cl

D. H. French
CSIRO, Lucas Heights Science and Technology Centre,
P.M. Bag 7,
Bangor, NSW 2234, Australia

R. W. King
Mérida 1948, Parque Residencial Laguna Grande,
San Pedro de la Paz, Chile

J. C. Ayers
Department of Geology, Vanderbilt University,
P.O. Box 105B, Nashville, TN 37235, USA

Introduction

In the supergiant El Teniente Cu–Mo deposit, Chile, the role of the low-grade to barren felsic porphyries occupying the core of the deposit, is still a matter of debate (Skewes and Stern 2007; Cannell et al. 2007). These small dacitic porphyries, formerly considered as the source of the ore fluids (Howell and Molloy 1960; Ossandón 1974; Camus 1975; Ojeda et al. 1980; Cuadra 1986), have recently been interpreted to play little or no part in the mineralization process, except for remobilizing pre-existing Cu mineralization associated to their mafic wallrocks (Skewes et al.

2002; Skewes and Stern 2007). Therefore, it was suggested that the El Teniente deposit should be classified as a breccia-type rather than a porphyry-type deposit, since the bulk of the copper ore is emplaced in breccia complexes in mafic rocks, which subsequently became the wallrock for later, post-ore, felsic porphyries. However, isotopic studies showing overlapping molybdenite Re–Os and zircon U–Pb ages (Maksaev et al. 2002, 2004; Munizaga et al. 2002; Cannell et al. 2003), ore petrography showing Cu–Fe sulfide zonation patterns related to the felsic porphyries (e.g., Camus 1975; Cannell et al. 2005, 2007), and LA-ICP-MS micro-analyses of fluid inclusions (Klemm et al. 2007) support the traditional view that the fluids and metals were focused through several small plugs, apophyses and dikes, i.e., the felsic porphyries, sourced from deeper levels. Both contrasting models nevertheless agree that the El Teniente deposit represents a huge hydrothermal ore system linked to a magma source at depth.

In this work, we present integrated petrographic, EPMA and PIXE data on hydrothermal rutile from felsic porphyries and their mafic wallrocks of the El Teniente deposit. The mineralogy, texture, chemistry (Mo and Sb), and origin of rutile is discussed in the aforementioned debated context. Besides, evidence of magmatic anhydrite in the felsic porphyries is presented and implications regarding the timing of volatile exsolution are discussed.

Texturally controlled samples, prepared as polished thin sections, are used instead of the traditional mineral concentrates. This working approach allows a better data integration offering the possibility of a process-based interpretation in a magmatic–hydrothermal context. Finally, the link between felsic porphyries and ore deposition is evaluated in light of the new rutile data.

Deposit geology

The El Teniente deposit is located in the Andes foothills of central Chile (34°S), ~50 km to the west of the present-day active volcanic chain. District geology is dominated by Miocene volcanic rocks (Farellones Formation) locally intruded by intrusives of intermediate composition (Kay et al. 1999). In the mine area, the magmatic activity is mainly represented by a volcanogenic mafic sequence intruded by relatively small felsic porphyries (Ossandón 1974; Camus 1975; Skewes 2000; Fig. 1). The larger Sewell complex, a quartz–diorite–tonalite–trondhjemite suite (Guzmán 1991; Reich 2001), is a pre-mineralization intrusion present outside of the high-grade ore zone in the southeastern sector of the deposit (Fig. 1). The small intrusives do not commonly outcrop on surface but underground observation indicates that they consist of a variety of shapes from vertically elongated stocks, dike-like bodies or apophyses to pipes. These metaluminous rocks are of leucocratic appearance, have a dominantly intermediate composition (60–70 wt.% of SiO_2) and are classified as Na-rich "I" type granitoids (Rabbia et al. 2001).

Characteristic textural elements associated to cupola environments, such as unidirectional solidification textures (USTs), were described in logged drill holes from some of the dacite pipes located eastward from the central dacite intrusion (Cannell et al. 2005). These USTs were interpreted to have formed contemporaneously with early wavy-edged quartz veins within a partly solidified hydrous igneous melt (Cannell et al. 2005), implying a close link between early veining events and the crystallization of these felsic porphyries under fluid saturation conditions.

At least five intrusive episodes of felsic magmas associated to mineralization were recognized within the deposit (Maksaev et al. 2002, 2004). Although the sequence of intrusion varies slightly according to zircon-overgrowth interpretations given by various authors, the general sequence of ore-related magmatic events may be summarized as follows (Maksaev et al. 2002, 2004; Cannell et al. 2005): the oldest magmatic activity is represented by zircon cores widely distributed in the eastern "quartz eye"-bearing felsic apophyses and pipes (6.46±0.11 to 6.11±0.13 Ma). A second magmatic pulse is represented by zircon-overgrowth ages (5.67±0.19 to 5.48±0.19 Ma) from these eastern dacite pipes. A third magmatic pulse is represented by the El Teniente dacite porphyry (5.28±0.10 Ma), a composite dike-like body of porphyritic dacite (Rojas 2002). The dacite ring dikes (4.82±0.09 Ma) surrounding the Braden pipe represent a fourth event and the final intrusive event related to mineralization is represented by minor porphyritic dacite (latite) intrusions and dikes (4.58±0.10 to 4.46±0.10 Ma; Fig. 1). Located in the center of the deposit, is an explosive vent structure known as the Braden breccia pipe (Fig. 1), a huge (>1.5 km in diameter) diatreme possibly related to the emplacement of late latite dikes (Camus 1975). Two post-mineralization lamprophyre dikes constitute the youngest intrusions (3.8 to 2.9 Ma; Cuadra 1986) within the deposit. All these intrusives were emplaced within a basaltic (47–54 wt.% SiO_2) subvolcanic sequence of late Miocene age traditionally known as "mine andesites". These mafic wallrocks composed of gabbros, diorites, and dolerites with volcaniclastics intercalations belong to the Farallones Formation (Skewes et al. 2002).

Irrespective of the dominant style of mineralization, i.e., breccia complexes (Skewes et al. 2002, 2005; Skewes and Stern 2007) versus vein stockworks (Cannell et al. 2005, 2007), both mineralized features are intimately related to each other (Skewes et al. 2002; Cannell et al. 2005) allowing to consider the El Teniente as a porphyry-type copper deposit. The deposit has a historic production plus remaining resources of 12.5 Gt at 0.63% Cu, 0.02% Mo (Sillitoe and Perelló 2005), and is the largest Cu concen-

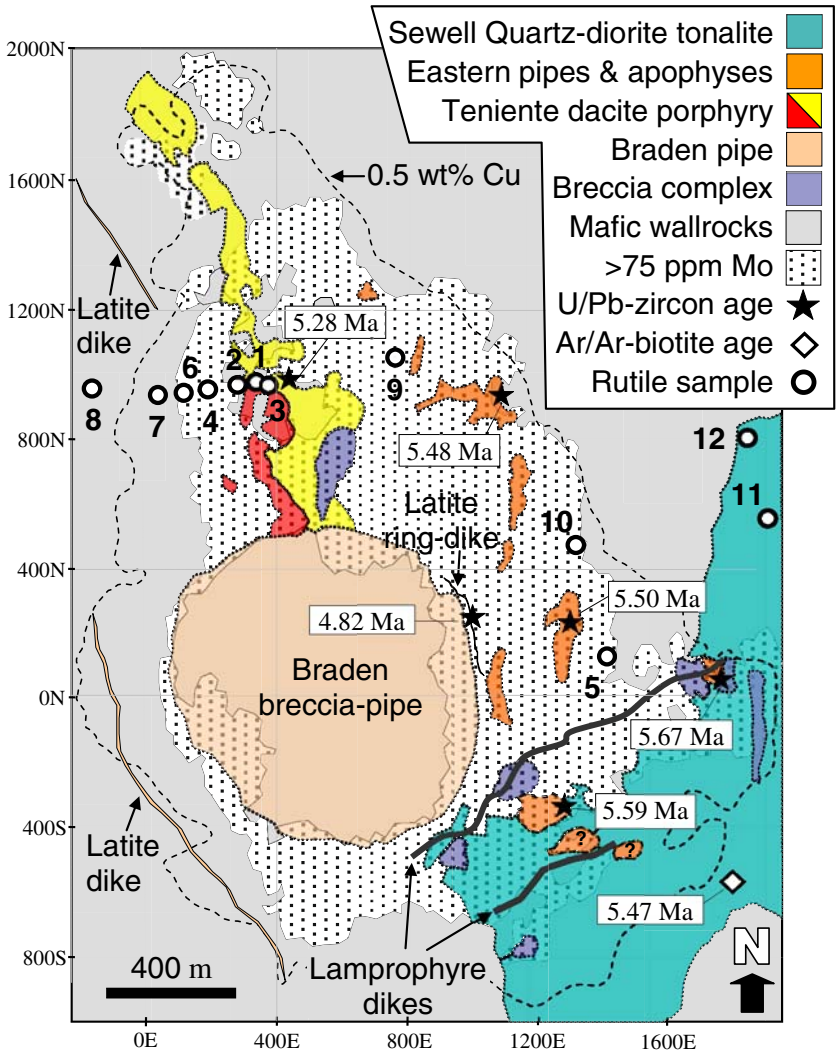

Fig. 1 Simplified geology of Ten-5 level (2284 m.a.s.l.) of the El Teniente deposit showing the location of rutile samples and ages of the magmatic units. The economic limit of the ore deposit (0.5 wt.% Cu) and Mo ore grade (>75 ppm; *dotted area*) are also shown. Modified after the El Teniente mining plans. Local coordinates in meters

tration in a single deposit in the Earth's crust. This huge orebody (~7 km^3) containing high-grade hypogene Cu–Mo sulfide mineralization is largely (>80%) hosted within the mafic wallrocks (Camus 1975; Fig. 1).

Hydrothermal alteration and mineralization

Since the origin of rutile in ore deposits is intimately related to hydrothermal alteration, a brief overview of the protracted hydrothermal history of the El Teniente deposit is presented next.

The hydrothermal evolution of this deposit has traditionally been divided into three main stages of alteration and hypogene mineralization: (1) late magmatic stage associated with potassic alteration; (2) main hydrothermal stage indicated by superimposed veining with quartz–sericite halos; and (3) late hydrothermal and post-ore stage represented by quartz–sericite alteration related to the marginal breccia surrounding the Braden pipe, the Braden pipe itself, and the tourmaline breccia in the carapace of the Sewell stock (Howell and Molloy 1960; Camus 1975; Ojeda et al. 1980). This traditional view, assuming a continuum from an early potassic stage followed immediately by the development of quartz-sericitic alteration, is challenged by the combined U–Pb, Re–Os, ^{40}Ar–^{39}Ar and fission-track apatite age evidence favoring a multistage evolution (Maksaev et al. 2004). The close agreement of Re–Os molybdenite and U–Pb zircon ages and the partial overlap with ^{40}Ar–^{39}Ar biotite and sericite ages suggest that the deposit was generated by five mineralizing events (~6.3; ~5.6; ~5.0; ~4.8, and ~4.4 Ma) directly associated with the crystallization of each felsic intrusive pulse (Maksaev et al. 2004). The resulting lifespan of the ore-forming system is about 2 Ma.

The earliest hydrothermal activity (early magnetite veins and early phyllic-tourmaline veins and alteration assemblages) was not associated with sulfides (Skewes et al. 2002; Cannell et al. 2005). This pre-mineralization alteration stage

is related to the intrusion of the Sewell diorite (Cannell et al. 2005). The ore depositional events are related to the younger dacite intrusions. The three earliest events are mainly associated with potassic alteration, whereas the fluids responsible for the fourth event generated both potassic and quartz–sericite alteration. The final ore depositional event appears to be exclusively related to quartz–sericite alteration (Maksaev et al. 2004). According to Klemm et al. (2007), the last three events represent just one major but extended event (~0.7 Ma) of mineralization associated to hydrothermal alteration evolving from potassic to quartz–sericite. Isotopic studies suggest that the potassic as well as the phyllic alteration events are largely if not exclusively related to magmatic fluids (Kusakabe et al. 1984, 1990; Skewes et al. 2001, 2002).

The vein stockwork domains resulting from these mineralizing events show variable degrees of hydrothermal overprint, as seen by widespread quartz–sericite overprinting previous potassic alteration (Skewes et al. 2002). An important aspect of the vein stockworks is that of the 14 vein stages recognized in this deposit, all but the first two (pre-mineralization stage) and the last (post-ore stage) contain Cu–Fe sulfides (Cannell et al. 2005). Molybdenite is present in all Cu-bearing veins and breccias except one wavy-edged, rare vein-type in dacite intrusives and two uncommon crackle breccias, one associated with dacite porphyry contacts and the other related to the marginal breccia of the Braden pipe (Table 5, Cannell et al. 2005).

Although breccia complexes are a characteristic feature of the El Teniente deposit, their classification and chronological sequence is not always rigorous because some were formed by multiple events (Skewes et al. 2002). The closely related but better constrained vein stockworks allow a better reconstruction of the thermal evolution of this huge deposit (e.g., Maksaev et al. 2004; Cannell et al. 2005).

Sampling strategy, rutile selection criteria and analytical methods

Drill-core sampling encompasses a 600-m high by 1,200-m wide section of the El Teniente deposit, including the main lithologies, alteration types, and different ore grades (Figs. 1 and 2; Table 2). Most samples (seven out of 12), however, are related to the major, contemporaneous, and long-lasting hydrothermal alteration and mineralization event related to the intrusion of the younger Teniente dacite and late dacite-latite porphyries.

Samples with rutile related to potassic alteration associated with the eastern dacite pipes and the El Teniente dacite porphyry intrusions frequently present superimposed phyllic alteration. The composition of rutile grains from well-defined phyllic veinlets is thought to represent the signature of fluids related to quartz–sericite alteration, mainly associated with the emplacement of late dacite intrusives (ring dikes and deeper intrusions underlying the Braden pipe). Finally, the composition of rutile from the deposit fringe may stand for fluid chemistry related to the evolution of hydrothermal solutions towards the outer portions of the deposit dominated by propylitic alteration. Rutile from the breccia-bodies in mafic wallrock was not included in this work.

All rutile grains analyzed in this study are from polished thin sections. Trace-element concentrations of rutile were obtained using the proton microprobe of the Heavy Ion Analytical Facility at the CSIRO Division of Exploration and Mining (Australia). A 3-MeV proton beam was used, focused into a ~1-μm beam spot. Data were analyzed using the GeoPIXE II analysis software (Ryan et al. 1990). Spectra were accumulated for a total integrated charge of 1 μC using a beam current of 3 nA which typically gave a count rate of 2,000 c/s. For each sample, reported data are averages for generally three to fifteen spots of several rutile grains. The precision of the proton microprobe data is given by the statistical uncertainty (e.g., standard error of ±1σ in Table 2); the accuracy has been established on the basis of analysis of standard materials which show differences of less than 5% relative to concentrations more than two to three times the detection limits. Full analytical conditions and data reduction methods are described in Ryan et al. (1990).

The Mo mapping image was obtained at the PIXE facility of the Materials Research Group, iThemba LABS (Somerset West, South Africa) under similar analytical conditions as for the Australian PIXE (3 MeV proton beam; ~1 μm beam spot and beam current of 3 nA) and using the same analysis software for data processing.

All rutile grains were previously characterized by electron microprobe analysis, using a 15 MeV and 50 nA electron beam focused into a ~1 μm beam spot (Rabbia 2002). This step proved particularly useful in selecting grain areas for PIXE analysis in the commonly compositionally zoned rutiles.

Hydrothermal rutile: origin and occurrence

Hydrothermal rutile from the El Teniente deposit is typically deep reddish-brown in color (Fig. 3a), varies from anhedral to euhedral in shape and is commonly fine-grained (10–50 μm), but larger crystals up to 600 μm have also been observed. Large rutile crystals usually show well-developed zoning patterns including patchy, oscillatory, and sector zoning (Fig. 3b).

Rutile formation in porphyry copper systems is coeval with hydrothermal alteration and results from the breakdown of Ti-rich minerals (Williams and Cesbron 1977; Czamanske et al. 1981; Beane and Titley 1981; Force 1991). This origin suggests that TiO_2, the major oxide

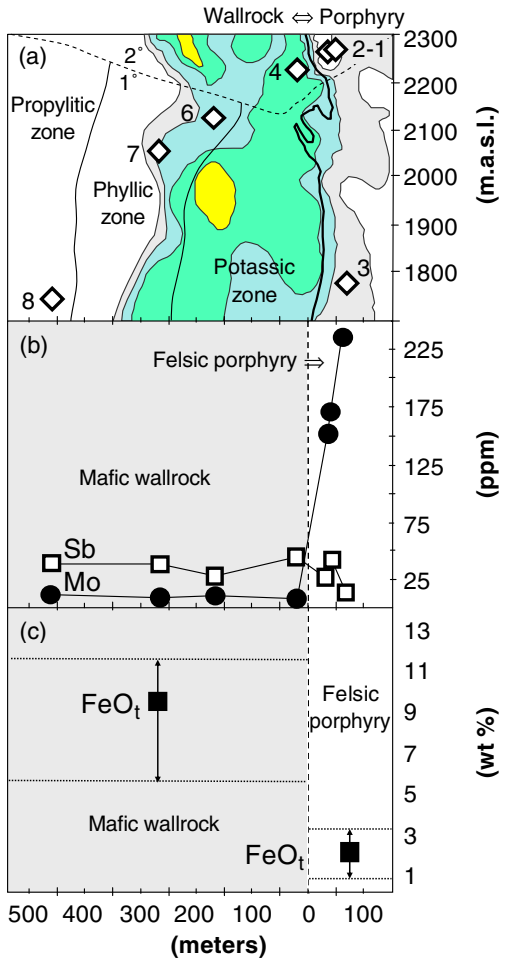

Fig. 2 **a** Vertical E–W section (650×600 m) of the northern part of the El Teniente deposit showing sample distribution; alteration (potassic, phyllic, and propylitic) and mineralization (*1°* hypogene; *2°* supergene) zones. Also shown are the porphyry-wallrock contacts (*bold full line*) and Mo ore grades. Modified after the El Teniente Division mining sections. **b** Mo and Sb contents of rutiles across the felsic porphyry-mafic wallrock contact. **c** Range (*horizontal dotted lines*) and mean FeO_T wt.% content (*filled squares*) in both rock units. Horizontal axis is similar in all three diagrams

constituent of rutile, is mainly inherited from the host rock, consistent with the general insolubility shown by TiO_2 both at near-surface conditions and in saline fluids at high temperatures (e.g., Ayers and Watson 1993). Thus, the TiO_2 content in the bulk rock is one of the factors limiting the amount of rutile potentially generated during alteration processes. At El Teniente, the Ti content of the felsic porphyries (~0.5 wt.% TiO_2) and the mafic wallrocks (~1.0 wt.% TiO_2; Table 1) suggests that more rutile can be expected to develop in the mafic rock unit. However, under potassic alteration conditions, the mafic wallrocks are selectively biotitized (Skewes et al. 2002) limiting Ti availability to form residual rutile in these rocks, since hydrothermal biotite may contain up to 3–4 wt.% of TiO_2. Therefore, fluid composition is another factor controlling rutile formation.

Another aspect to consider is that rocks with contrasting compositions may also have different Ti-rich phases (e.g., biotite, titanite, ilmenite, etc.), which may also imply different chemical stabilities for the precursors minerals from which rutile may form.

The primary Ti-rich minerals from the El Teniente felsic porphyries include biotite and minor hornblende along with accessory magnetite, titanite ± ilmenite. Over 85% of the whole-rock TiO_2 content (~0.4 wt.%; Table 1), however, is controlled by only two phases: biotite and titanite (Table 3). While the relative modal proportion of each Ti-bearing mineral varies from quartz diorite to dacite porphyries, its total amount, represented by the color index of these rocks, is relatively low and constant, ranging from 6 to 12 wt.% (Reich 2001; Rojas 2002). For most mafic wallrocks, ferromagnesian silicates and Fe–Ti oxides constitute the main primary Ti-rich minerals, although their relative modal proportions are difficult to estimate due to the pervasive hydrothermal alteration (Skewes and Arévalo 2000).

The chemical stability of the primary Ti-rich minerals is particularly affected by high-temperature, SO_2-rich oxidizing fluids (e.g., Udubasa 1982; Force 1991; Haggerty 1991). In the felsic porphyries, such fluids promoted oxidation-induced breakdown of titanite during potassic alteration events, generating residual rutile (e.g. titanite + SO_2-rich fluid ⇒ anhydrite + quartz + rutile; Fig. 3c). Additionally, minor quantities of rutile were also formed in felsic porphyries by magmatic biotite re-equilibration during potassic alteration (needle-like "sagenitic" rutile; Fig. 3d). Magmatic Ti-magnetite also re-equilibrates to Ti-poor magnetite during this hydrothermal event, releasing additional Ti for rutile formation. Within the mafic wallrocks, hydrothermal rutile formed during potassic alteration is mainly derived from accessory Fe–Ti oxides.

Biotite, stable in early domains of potassic alteration, is partially replaced by a sericite–quartz–chlorite–rutile association during subsequent widespread phyllic alteration. In strongly phyllic-altered intervals of the dacite porphyries, most whole-rock TiO_2 is present as fine-grained rutile associated with or in halos around veins developed during quartz-sericitic alteration. In distal propylitic zones within the mafic wallrocks, tiny amounts of rutile are mainly found along with secondary sphene as patches in partially altered ilmenite (Fig. 3e) and also as discrete grains associated with chlorite and epidote.

In summary, superimposed episodes of different alteration processes (mainly potassic and phyllic) acting on contrasting lithologies (felsic and mafic), produced different generations of hydrothermal rutile from different precursor mineral phases. Potassic alteration events, largely associated with the emplacement of both the eastern dacite pipes and apophyses and the El Teniente dacite porphyry were titanite

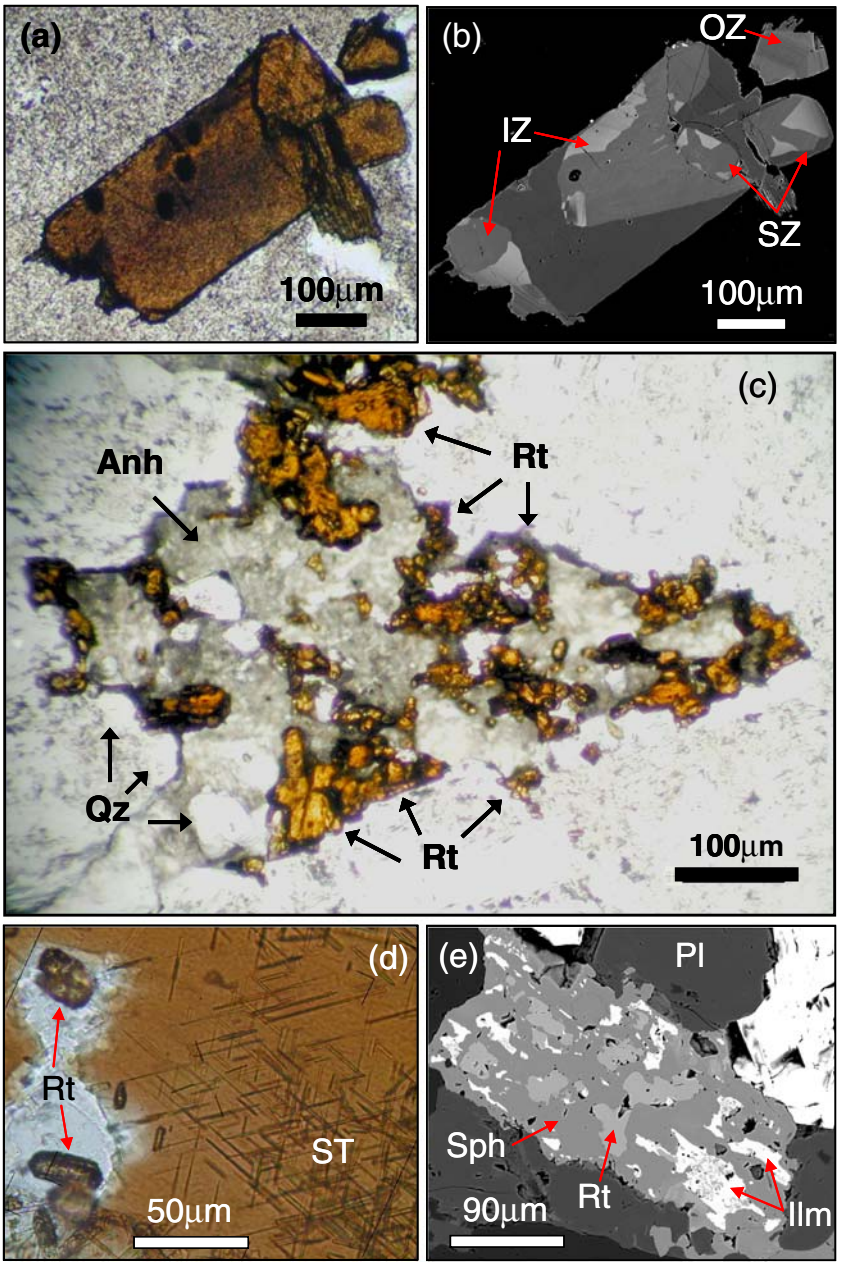

Fig. 3 **a** View in plane-polarized light (ppl) of a large rutile grain, from eastern dacite pipes. Note the reddish-brown coloration and the subhedral shape. **b** Backscattered electron (BE) image of the same crystal showing the heterogeneous chemical composition (zonation pattern) resulting from the combination of sector zoning (*SZ*), oscillatory zoning (*OZ*) and irregular or patchy zoning (*IZ*). Brighter areas represent sectors with higher trace element contents. **c** Rutile, quartz, and anhydrite pseudomorphs after magmatic titanite from the El Teniente dacite porphyry (ppl). **d** Biotite phenocryst from the El Teniente dacite porphyry showing needles of rutile or sagenitic texture (*ST*) and more equant rutile crystals (*Rt*) in a chloritized area of the biotite (ppl). **e** BE image of magmatic ilmenite breakdown showing patches of anhedral rutile (*Rt*), titanite (*Sph*), and relictic ilmenite (*Ilm*) from Sewell diorite in the propylitic zone. *Pl* plagioclase and *Mt* magnetite

(±hornblende ± ilmenite)- but not magnetite- and biotite-destructive; while later quartz–sericite events, related to late dacite ring dikes and intrusions underlying the Braden pipe, were mainly biotite-destructive.

The rutile polymorph anatase was also identified at El Teniente, but its occurrence is rare and tends to be restricted to late carbonate veinlets located on the fringe of the deposit where propylitic alteration dominates (Rabbia et al. 2003).

Analytical results

Results of PIXE spot analyses for Mo and Sb concentrations in rutile are summarized in Table 2. A complete data list of PIXE analyses (n=85) and drillhole information are included in the Supplementary Data Repository. PIXE elemental mapping shown in Fig. 4 reveals a crystallographic control (e.g., sector zoning) of Mo distribution in hydrothermal rutile. EMP analyses of rutile from El Teniente show relatively high total minor- and trace-element contents ranging from 1 to 14 wt.% (mean ~3 wt.%, n=326), with Fe, W, and V accounting for almost 90% of the minor element content (Rabbia 2002).

In the deposit core, regardless of the alteration event, the mean Mo content of rutile from felsic intrusives (186± 20 ppm; n=42) is ~35 times higher than in rutile from wallrocks (5.4±1.1 ppm; n=17; Table 2). In contrast, the

Table 1 Summary of compositional data for the mafic wallrocks and felsic porphyries

Oxides	Wt. (%)					
	Teniente porphyry[a]		Sewell diorite[b]		Mafic wallrock[c]	
	Mean	Range	Mean	Range	Mean	Range
SiO_2	64.3	66.4–62.6	63.2	65.6–60.6	50.1	53.6–46.6
TiO_2	0.41	0.50–0.34	0.54	0.62–0.45	1.09	1.22–0.88
FeO $_{Total}$	1.98	3.08–0.71	3.27	3.74–2.80	9.53	11.69–5.99
DI	79.2	83.7–75.3	70.8	76.1–68.4	34.8	40.4–28.9

All data from Rabbia (2002)

DI Thornton and Tuttle differentiation index

[a] Includes all varieties of the El Teniente dacite porphyry. Number of samples: 17

[b] Excludes varieties from the dacite apophyses and ring dikes. Number of samples: six

[c] Includes different varieties of mafic wallrocks. Number of samples: 16

mean Sb content in rutiles does not vary significantly with rock type: 35±3 ppm Sb (n=42) in rutile from porphyries versus 27±4 ppm Sb (n=17) in rutile from wallrocks (Table 2; Fig. 5). Remarkably, Mo-poor rutile is present in Mo-rich mafic wallrocks (>75 ppm Mo) whereas Mo-rich rutile is hosted by Mo-poor felsic intrusive rocks (commonly <75 ppm Mo). Variation in Mo content between rutile crystals from different host rocks disappears outside the high-grade ore zone, where most rutile has similar but low Mo contents (3.5±0.8 ppm; n=26; Table 2).

Despite the few samples analyzed for such a giant deposit, a consistent picture of spatial variation of metal

Table 2 Summary of Mo and Sb contents and Mo/Sb ratios in rutile measured by PIXE

Sample	Ore[a]		Rock		Mo (ppm)	Sb (ppm)	Mo/Sb	n
	Grade	Type	Type	Alteration	Mean ± s.e.	Mean ± s.e.		
1	Low	S	Dacite porphyry	Potassic / phyllic	170±139	14±3	12.14	4
2	Low	S	Dacite porphyry	Potassic	153±38	42±6	3.64	9
3	Low	H	Dacite porphyry	Phyllic	236±26	25±4	9.44	15
4	High	S	Mafic rock	Potassic	6.3	44	0.14	1
5	High	H	Mafic rock	Phyllic	4.9±0.7	17±3	0.29	8
6	High	H	Mafic rock	Potassic	9.3±3.9	28±7	0.33	8
7	High	H	Mafic rock	Phyllic	2.4±1.8	39±9	0.06	4
8	Low	H	Mafic rock	Propylitic	4.2±2.2	39±7	0.11	7
9	Low	H	Dacite apophyses	Potassic	151±33	53±5	2.85	11
10	Low	H	Dacite apophyses	Potassic	190±87	31±10	6.13	3
11	Low	H	Tonalite	Propylitic	3.8±1.7	45±12	0.08	7
12	Low	H	Tonalite	Propylitic	3.0±1.0	46±7	0.07	12
			All porphyries(samples 1–3, 9, 10)	Potassic	169±28	43±4	3.93	25
				Phyllic	212±28	24±4	8.83	17
			All wallrocks(samples 4–8, 11, 12)	Potassic	8.7±3.1	31±6	0.28	5
				Phyllic	4.0±0.8	25±5	0.16	12
				Propylitic	3.5±0.8	44±5	0.08	26
			Porphyries (all alteration types)		186±20	35±3	5.31	42
			Wallrock (all alteration types)		4.3±0.7	37±3	0.12	43
			Wallrock (propylitic excluded)		5.4±1.1	27±4	0.20	17

[a] Ore grade is divided into: high (Mo >75 ppm) and low (Mo <75 ppm). Ore type is divided into: hypogene (H) and supergene (S).

s.e. standard error

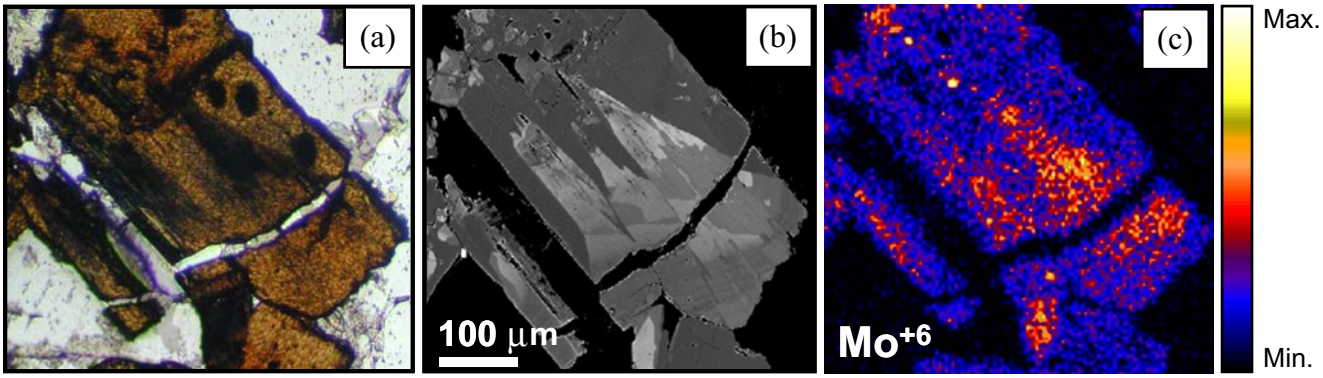

Fig. 4 **a** View of a large rutile crystal from the eastern dacite pipe. The darker areas correspond to sectors of high trace element content (ppl). **b** BE image of the same grain showing sector zoning where brighter areas relate to high trace element concentrations. **c** PIXE elemental mapping showing crystallographic control (sector zoning) on Mo distribution in the same rutile grain. *Color scale* shows relative maximum (*Max*) and minimum (*Min*) Mo contents

content in rutile emerges. This Mo-in-rutile distribution pattern suggests a causal relationship with precipitation of Mo-bearing sulfides.

Crystal chemistry of Mo-bearing hydrothermal rutile

Although molybdenite (MoS_2) is by far the major Mo carrier in the El Teniente deposit, Mo is also incorporated into hydrothermal rutile with concentrations of up to ~600 ppm (Supplementary Data Repository). PIXE elemental mapping in rutile (Fig. 4) reveals that Mo is differentially partitioned among non-equivalent crystallographic faces, thereby related to growth sector zoning in the rutile crystal. This crystallographic control on Mo incorporation into the rutile structure rules out the possibility that MoS_2 micro-inclusions may be the source of measured Mo in hydrothermal rutile. Furthermore, the presence of sharp compositional gradients (e.g., sector and oscillatory zoning; Fig. 3b) implies that ionic diffusion is minor and that the original trace-element content of rutile is preserved despite the long thermal history of the deposit.

Since Ti^{4+} cannot be directly replaced by Mo^{6+}, a charge-balancing substitution mechanism has to be considered for its incorporation into the rutile structure. It is worthy to note that Mo may also be regarded as a high field-strength element (HFSE; e.g., Fitton 1995; O'Neill and Eggins 2002) and thus it may behave as other HFSE (e.g., Nb^{5+}, Ta^{5+}), i.e., replacing Ti^{4+} in octahedral sites via coupled substitution. In this case: $^{VI}Mo^{6+}+2\,^{VI}M^{3+} \Leftrightarrow 3\,^{VI}Ti^{4+}$, where M^{3+} in hydrothermal rutile from El Teniente is mainly Fe (Rabbia 2002).

Antimony, the other trace element considered here, is largely present as tennantite–tetrahedrite$_{ss}$ ± stibnite (Cannell et al 2005). Rutile, however, also concentrates Sb, but only up to ~100 ppm (Supplementary Data Repository). Like Mo, this chalcophile element (Mason 1966) may also act as an HFSE (Zack et al. 2002; Hattori and Guillot 2003) and thus replaces Ti^{4+} in the rutile structure via coupled substitution:

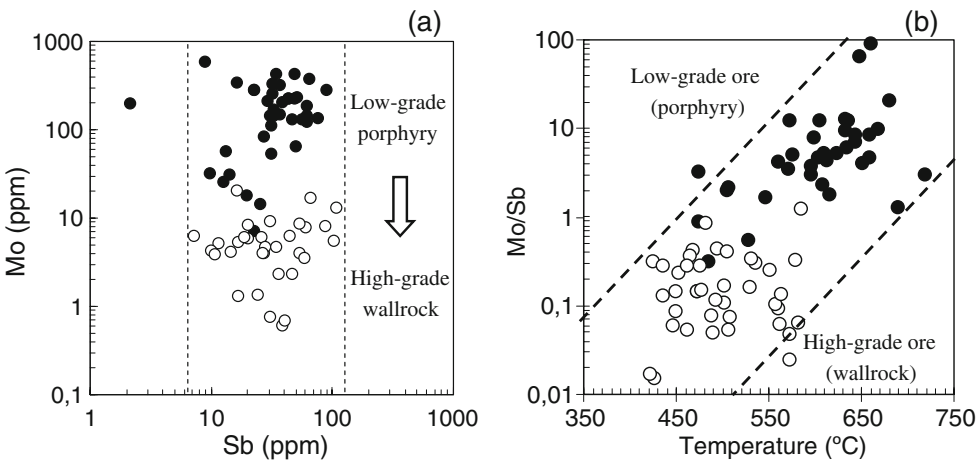

Fig. 5 **a** Co-variation diagram of Mo and Sb contents in rutile from El Teniente. *Filled circles* represent porphyry-hosted rutiles and *open circles* wallrock-hosted rutile. **b** Mo/Sb for rutile samples in high- and low-ore grade zones versus temperature. Symbols as in **a**

$^{VI}Sb^{5+}+{}^{VI}M^{3+}\Leftrightarrow 2{}^{VI}Ti^{4+}$, where M^{3+} is again mainly Fe (Rabbia 2002).

The variation of Mo and Sb contents in the rutile samples is remarkably different; while Sb remains essentially constant, Mo decreases towards the cooler wallrocks (Fig. 5a,b). Experimental evidence demonstrates that Mo in fluid-equilibrated rutile may attain the weight % level in high-temperature, S-free hydrothermal systems (Rabbia 2002), thus local changes in $a_{(H2S)}$ of natural systems may affect Mo behavior (see next section). If similar controls operate for Sb, changes in the Mo/Sb ratio may thus be highlighting the role of the solubility difference between the potential Mo and Sb sinks.

Redox state, sulfur speciation, and Mo behavior

Knowledge of the redox state or oxygen fugacity (fO_2) of magmatic–hydrothermal systems is important because it controls the speciation of S (Carroll and Rutherford 1985) which, in turn, influences the geochemical behavior of Mo. The presence of biotite ± hornblende, magmatic anhydrite, S-enriched apatite (up to 1 wt.% SO_3), accessory magnetite and titanite, the absence of Eu anomalies in bulk-rock REE patterns and the leucocratic character of the El Teniente porphyries (Rabbia et al. 2000; Reich 2001; Hernández et al. 2002, 2004) indicates that the magmas from which they crystallized were hydrous, oxidized, and sulfate-saturated.

The presence of magmatic anhydrite only as micro-inclusions in primary phenocrysts (Fig. 6a,b), suggests that either non-armored anhydrite from the rock matrix was leached out during the hydrothermal stage, given its high solubility in hot saline aqueous fluids (e.g., Blount and Dickinson 1969), or that anhydrite formation during groundmass crystallization was precluded by fluid exsolution, owing to high S partitioning into low-pressure, high-temperature, and oxidized aqueous fluids (e.g., Scaillet et al. 1998). In any case, the evidence indicates that these magmas were sulfate-saturated, suggesting that sulfur from both the melt and the separate sulfate phase may have contributed to the deposit formation as in other giant hydrothermal ore deposits (e.g., Chambefort et al. 2008).

The coexistence of anhydrite with plagioclase, hornblende, and biotite constrains the fO_2 of felsic magmas to ≥NNO+1.3 (e.g. Scaillet and Evans 1999). Under these conditions, most S in the silicate melt is present as SO_4^{2-} (Carroll and Webster 1994) whereas in the exsolved fluid phase it is mostly present as SO_2 (Carroll and Rutherford 1985; Carroll and Webster 1994).

Anhydrite micro-inclusions in plagioclase phenocrysts were only found in their rims (Fig. 6b) implying that the sulfate-saturated condition was reached before groundmass crystallization. The timing of sulfate formation suggests that the magma was not saturated with respect to a volatile phase; otherwise S would strongly be partitioned into the fluid phase ($D_S^{fluid/melt} \sim 1000$; fluid/melt partition coefficient for dacite melts; Scaillet et al. 1998).

Under the high fO_2 prevailing in such a magmatic–hydrothermal system, the dissolution of Mo in silicate melts and aqueous phases is almost entirely as Mo^{6+} (Candela and Holland 1984; O'Neill and Eggins 2002). High fO_2 improves the efficiency of Mo removal from silicate melts into aqueous phases (Candela and Bouton 1990) and along with high salinities and temperatures increases its solubility in ore-forming fluids (Cao 1989; Ulrich and Mavrogenes 2008).

Since Mo precipitates in porphyry copper deposits mainly as MoS_2, its incorporation into an oxide phase (rutile) may be indicative of local and/or temporal low $a_{(H2S)}$ conditions likely associated to relatively high temperature and/or high fO_2. Such conditions may lead to

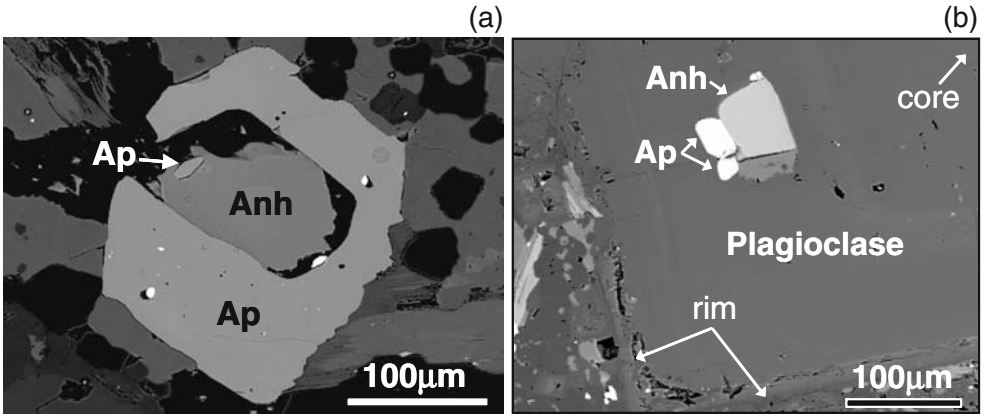

Fig. 6 **a** BE image of co-crystallized magmatic apatite (*Ap*) and anhydrite (*Anh*) from the El Teniente dacite porphyry. Note that the Anh also includes a euhedral Ap grain (*white arrow*). Despite the partial dissolution of the Anh crystal (*black areas*), probably due to hydrothermal alteration and/or sample preparation, euhedral outlines are well preserved. **b** Detail of a large plagioclase phenocryst (*rock matrix towards the left and bottom of the photomicrograph*). Trapped euhedral crystals correspond to Ap and Anh

the formation of low-grade or barren core zones of porphyry deposits (Lowell and Guilbert 1970). Therefore, ambient conditions may be as relevant as metal availability in rutile chemistry.

Mo contribution from Ti-rich parental phases

During the crystallization of silicic magmas, Mo can be partitioned into Ti-bearing accessory phases such as ilmenite, magnetite, titanite, and biotite (Luhr et al. 1984; Candela and Bouton 1990; Stimac and Hickmott 1994; Candela 1997; Piccoli et al. 2000). Mo present in hydrothermal rutile may therefore be inherited from precursor magmatic phases. This could offer a straightforward explanation concerning the presence of Mo-rich rutiles in porphyries as well as for the sharp decrease in Mo content of rutile across the contacts towards the mafic wallrocks.

The absence of an early event of volatile exsolution in the dacite porphyry (see previous section) suggests that at the crystallization time of titanite and biotite, the main precursor phases of rutile in the porphyries, most Mo was still present in the silicate melt fraction. Otherwise, under the high fO_2 (≥NNO +1.3) of the magma, Mo would be efficiently partitioned into the fluid phase owing to its relatively high $D_{Mo}^{fluid/melt}$ (Candela and Holland 1984; Candela and Bouton 1990; Keppler and Wyllie 1991). The extent of Mo captured by these early-crystallized Ti-rich phases depends essentially on their $D_{Mo}^{crystal/melt}$ and melt composition. Mo released after titanite and biotite breakdown may then be incorporated into residual rutile given the ease of Ti–Mo exchange (Ribbe 1982; Gunow 1983; Candela and Bouton 1990; Piccoli et al. 2000), particularly under fluid-dominated, high-temperature, oxidized and/or low $a_{(H2S)}$ conditions (Rabbia 2002).

A simple mass-balance calculation may help to make a first rough estimation of Mo-in-rutile potentially inherited from Ti-rich accessory phases. The major difficulty arises from the fact that Ti-rich magmatic minerals from these porphyries either did not survive high-temperature alteration (e.g., titanite) or their original compositions were modified (e.g., magnetite, biotite). Therefore, published data on Mo contents for representative Ti-rich accessory phases from less altered rocks but with a similar differentiation index DI were used (see details in Supplementary Data Repository). Results of the mass balance calculation are presented in Tables 3 and 4a–b.

Titanite and Ti-magnetite were considered as parental phases to evaluate the Mo content of rutile formed during potassic alteration in felsic porphyries. The calculations suggest that ~34% of the Mo in such rutile (57 ppm; Table 3) might be derived from parental titanite. A similar result (~30%) is obtained using other titanite compositions (see Supplementary Data Repository).

The results also show that despite the lower TiO_2 contribution from magnetite, its potential Mo input may represent ~70% (118 ppm; Table 3) of the measured Mo in rutile (169±28 ppm Mo; Table 2). The model TiO_2/Mo ratio (0.56) and the model mean Mo content (174 ppm; Table 4b) in rutile weighed by Mo contributions from titanite and magnetite accurately reflect the measured mean Mo content (169±28 ppm; Table 4b) and TiO_2/Mo ratio (0.57; Table 4b) of the rutile formed during potassic alteration. Although titanite is the dominant TiO_2 source (~77% of total TiO_2; Table 4a), magnetite may represent the major Mo supply for rutile (~67% of total Mo; Table 4a) due to the difference in TiO_2/Mo ratio and modal abundance (~1.3/~0.2 and 0.39 wt.%/0.94 wt.%, respectively; Table 3).

During subsequent phyllic alteration biotite instead of titanite is the main Ti source for the additional generation of rutile in porphyries. Due to the overprinting nature of the phyllic alteration, rutile associated to biotite breakdown coexists with rutile derived from titanite and magnetite. Therefore, the mean model value of Mo (327 ppm; Table 3) for phyllic-related rutile, calculated considering biotite as the only parental phase, does not fit well with the measured Mo value (mean 212±28 ppm Mo; Table 2). A more representative model mean Mo value results from weighing the participation of all rutile precursor phases (259 ppm; Table 3).

Despite the assumptions made and the limitations imposed by published data from other systems, the calculated (Table 3) and measured (Table 2) Mo values from all porphyry-hosted rutile samples are in relatively good agreement. The overall evidence suggests that during both potassic and phyllic alteration Mo from Ti-bearing magmatic parental phases has notably contributed to increase the Mo content of hydrothermal rutile from the El Teniente dacite porphyries.

In contrast, Mo contents in rutile from the Sewell tonalites from outside the economic limit of the deposit are notably lower (Table 2). These rocks, however, are less evolved (DI=68–76; Table 1) than the dacite porphyries from inside the deposit (DI=75–84; Table 1). Furthermore, most rutile in the tonalites formed from ilmenite owing to the stability of titanite during propylitic alteration (Fig. 3e) and the only mild chloritization of biotite of the rocks studied.

The model mean value of Mo in rutile (~14 ppm) calculated using published ilmenite data is ~4 times higher than that measured in rutile from Sewell tonalite (mean, ~3–4 ppm Mo, Table 1). The ilmenite data available for calculation are from rocks more evolved (DI=91) and reduced (fO_2<QFM) compared to the Sewell tonalite (DI=68–76, Table 2; fO_2≥NNO). These differences may cause an overestimation of the calculated Mo

Table 3 Mass-balance calculation of Mo derived from Ti-rich parental phases in hydrothermal rutile from the El Teniente dacite porphyry

Ti-rich mineral phases [a]						Whole rock (porphyry) [b]						Hydrothermal rutile				
Name	Mode[c]	TiO_2[d]	Mo (ppm) [e]		TiO_2/Mo	TiO_2		Mo (ppm)		Concentr. factor [f]		Mo content (ppm)			Mt, Sph, Bt proportion	Alteration
	wt %	wt %	Range	Mean		wt %	X_{TiO2}	Range	Mean			Mean [g]	Range [g]	Mean [h]		
Mt	0.94	4.7	8-35	24.7	0.2	0.044	0.103	0.075-0.328	0.231	Mt	20.6	510	165 - 722	118	0.231	Pot.
Sph	0.39	38.0	21-46	29	1.3	0.146	0.344	0.081-0.177	0.112	Sph	2.6	74	54 - 117	57	0.769	
Bt	5.48	4.3	3.3-29	14.5	0.3	0.236	0.553	0.181-1.589	0.794	Bt	22.6	327	74 - 654	327	1.000	Phy.
				Σ =		0.426	1.000	0.34 - 2.09	1.14			Mean[i]	Range [i]			
Mo content (ppm) in rutile from potassic alteration (Mt+Sph) →												174	54 - 722			
Mo content (ppm) in rutile from phyllic alteration (Bt) →												327	74 - 654			
Mo content (ppm) in rutile from both potassic and phyllic (Mt+Sph+Bt) →												259	77 - 477			

[a] *Mt* Ti-magnetite, *Sph* titanite, and *Bt* biotite

[b] The weight % (wt.%) and weight fraction (X_{TiO2}) and the range and mean Mo content contributed by each mineral phase to the whole rock. The grand total (∑) of 0.42 wt.% TiO_2 matches average whole-rock TiO_2 content of felsic porphyries (Table 2)

[c] Calculated from modal abundances in vol% after Rojas (2002)

[d] TiO_2 wt.% in Bt after Hernández (unpublished data), in Sph after Piccoli et al. (2000), and in Mt was estimated following Ghiorso and Sack (1991)

[e] Mo contents in Mt and Bt after Nash and Crecraft (1985) and in Sph after Piccoli et al. (2000). *n* numbers of values

[f] Concentration factor = $[Ti]_{rutile}/[Ti]_{Ti\text{-}rich\ phase}$. $[Ti]_{rutile}$ after Rabbia (2002)

[g] Calculated $[Mo]_{rutile}$ formed after Ti-bearing primary phases

[h] The $[Mo]_{rutile}$ weighted by the proportion of each Ti-rich phase involved during each alteration event

[i] The $[Mo]_{rutile}$ weighted by X_{TiO2} contributed by the sum of Ti-rich minerals involved in the respective alteration event.

value, given that Ti-bearing phases crystallizing from relatively reduced, high-silica melts are more prone to become Mo-enriched (Nash and Crecraft 1985; Tacker and Candela 1987; Candela and Bouton 1990). The lower temperature for distal propylitic alteration may additionally contribute to the observed discrepancy (see Discussion section). The presence of titanite associated with rutile as a product of ilmenite breakdown (Fig. 3e) may also help to explain the low Mo content of such rutile, since secondary titanite tends to be Mo-rich (up to ~50 ppm; Piccoli et al. 2000).

As mentioned previously, rutile from the basaltic wall-rocks (DI=40–29; Table 1) was mainly derived from the breakdown of Fe–Ti oxides. Due to the difficulty in establishing the abundance of accessory Fe–Ti oxides in these rocks, no attempt was made to calculate their Mo contribution to rutile. It can be anticipated, however, that the amount of Mo likely derived from these oxides should be even lower than that from the Sewell tonalites (DI=68–76; Table 1) because melt Mo contents (Candela and Bouton 1990) and $D_{Mo}^{crystal/melt}$ (Nash and Crecraft 1985) increase with melt differentiation.

Table 4 (a) Model TiO_2 and Mo contributions (in %) from Ti-rich parental phases and (b) model and measured TiO_2/Mo ratios and Mo contents (ppm) in rutile from the El Teniente porphyries

(a) TiO_2 and Mo contribution percentages

	Potassic + phyllic alt.		Potassic alteration	
	TiO_2	Mo	TiO_2	Mo
Mt	10.3	20.3	23.1	67.4
Sph	34.4	9.8	76.9	32.6
Bt	55.3	69.8	–	–

(b) Hydrothermal rutile

	Phyllic alt. (Bt)		Potassic alt. (Mt + Sph)	
	TiO_2/Mo	Mo (ppm)	TiO_2/Mo	Mo (ppm)
Calculated	0.30	327	0.56	174
Measured	0.46	212	0.57	169

The lack of representative data on Sb contents of Ti-rich magmatic phases precludes any estimation concerning the proportion of Sb in rutile derived from parental phases.

Discussion

Mo in hydrothermal rutile from dacite porphyries

LA-ICP-MS microanalyses of fluid inclusions from the El Teniente deposit indicate that the Mo contents in all except one of the 11 types of identified fluid inclusions are relatively low, between 10 to 50 ppm (Klemm et al. 2007). Minor post-entrapment H_2O loss suggests that the actual Mo values may be even lower (Klemm et al. 2007). An apparent $D_{Mo}^{rutile/fluid}$ partition coefficient ≥4 is obtained using these fluid inclusion data in order to attain the mean Mo contents in rutile of ~200 ppm (e.g., samples 1, 2, and 3; Table 2). This result contrasts with the $D_{Mo}{}^{rutile/fluid}$ value experimentally determined for hydrothermal rutiles (≤1.5; Rabbia 2002). However, if this smaller value is used instead, then Mo contents in the ore-forming fluids of ≥133 ppm would be required which is more than the Mo contents measured in fluid inclusions. The Mo sequestering process of Ti-rich phases during the magmatic stage may help to explain this apparent contradiction.

Early crystallization under oxidizing conditions of accessory titanite, Ti-magnetite, and biotite phenocrysts, coupled with relatively late exsolution of a magmatic volatile phase may have promoted Mo incorporation into these Ti-rich phases (see previous section). Subsequent re-equilibration (Fig. 3d) and/or breakdown (Fig. 3c) of these igneous Ti-rich minerals during hydrothermal alteration events leads to release of Ti and Mo from these phases. Given the low solubility of Ti in saline fluids at <700°C (Ayers and Watson 1993), most rutile will nucleate and develop at textural positions where previous Ti-rich phases were present, creating, in some cases, rutile-intergrowth pseudomorphs after their parental phases (Fig. 3c and e). These fluid-equilibrated rutile aggregates grow in a micro-environment locally enriched in Mo derived from Ti-rich phases, as suggested by the mass balance estimation (Table 4b). This close relationship between rutile and its parent phases may explain the relatively high Mo contents in rutile from the dacite porphyries, without invoking either unlikely large $D_{Mo}^{rutile/fluid}$ (≥4) or unusually high Mo contents (≥133 ppm) in the bulk fluid phase of the porphyry system.

Although Mo inherited from the parent mineral phases may help to constrain Mo provenance, the broad range of Mo abundances in the rutile samples analyzed (Table 2) requires further explanation. Using the Zr-in-rutile geothermometer (Tomkins et al. 2007), it is apparent that the Mo content in rutile is strongly dependent on temperature, varying by more than two orders of magnitude over a ~300°C temperature range (Figs. 7 and 8). The formation temperature of rutile suggests that MoS_2, precipitating at below ~550°C (Fig. 6f, Klemm et al. 2007), may not have co-crystallized with high-temperature rutile (>550°C; Fig. 7). Otherwise, Mo enrichment in rutile would not be feasible due to the chalcophile affinity of this element. Consequently, high-temperature (>550°C) hydrothermal rutile crystallizing in the porphyries may become enriched in Mo by incorporating most Mo released from Ti-rich phases as discussed previously. The relative timing of magmatic fluid exsolution may thus place constraints on the degree of Mo enrichment in rutile by limiting the amount of Mo incorporated in Ti-rich parent mineral phases. Knowing the timing of fluid phase evolution in the magmatic system, the impact that the different Ti-rich phases may have on the high-temperature rutile chemistry can be anticipated using their modal abundance and TiO_2/Mo ratios. For instance, estimations for porphyry-hosted rutile (Tables 3 and 4) suggest that although titanite was the major Ti source during early potassic alteration most Mo probably came from Ti-magnetite, and that during subsequent phyllic alteration, biotite was the main source of both Ti and Mo.

Although small amounts of magmatic sulfides may strongly control the storage and release of chalcophile metals (Larocque et al. 2000), the proportion of Mo controlled by these sulfides is considerably less (Keith

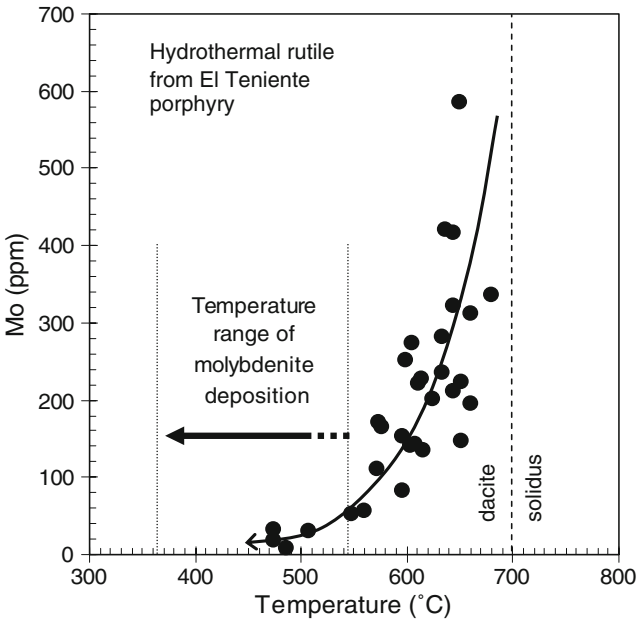

Fig. 7 Mo content versus formation temperature of rutile from the El Teniente dacite porphyry. The Zr-in-rutile geothermometer (Tomkins et al. 2007) corrected for a pressure of 120 MPa was used for temperature calculation. Temperature range of MoS_2 deposition is after Klemm et al. 2007. The dacite *solidus* close to H_2O-saturation is shown as reference

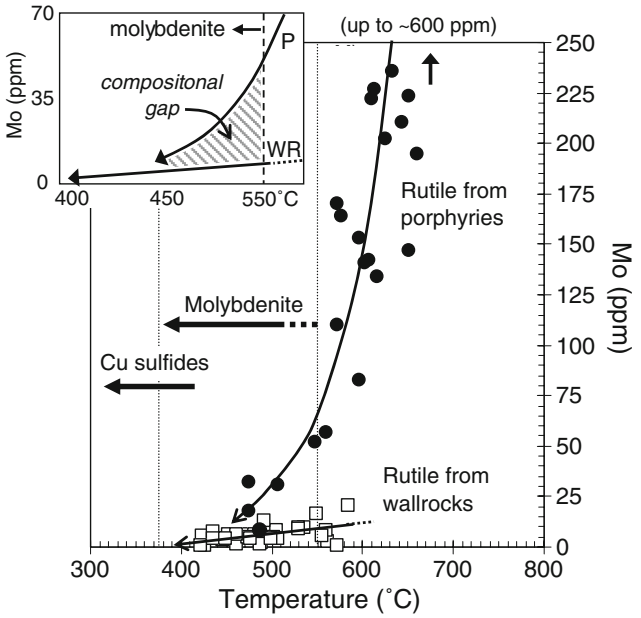

Fig. 8 Mo content versus formation temperature of rutile from the El Teniente dacite porphyry (*P*) and wallrocks (*WR*). Variation trends of Mo in rutile from P and WR and the compositional gap for the temperature range of molybdenite–rutile co-crystallization are also shown (*insert*). Deposition temperatures of Cu-sulfides and molybdenite are from Klemm et al. 2007. Formation temperature of rutile was calculated as in Fig. 7

et al. 1997). In oxidized felsic magmas, significant amounts of Mo reside in Ti-magnetite, sphene, and biotite (Piccoli et al. 2000), which after fluid exsolution is mostly transferred to high-temperature residual rutile and thus remains unavailable to the ore-forming fluids. The similarity between model and measured Mo contents in rutile (Table 4b) supports this view. Therefore, the finding of Mo-rich rutile in altered felsic porphyries emphasizes the importance of timing of volatile saturation for the efficiency of Mo extraction from oxidized, hydrous felsic melts.

Mo in hydrothermal rutile from mafic wallrocks

Low Mo contents in rutile from distal parts of the hydrothermal system can be expected due to the temperature dependence of Mo incorporation into the rutile structure (Fig. 7). The two different variation trends displayed by porphyry and wallrock rutile (Fig. 8), however, cannot simply be attributed to temperature control. Although the Mo contribution from Ti-rich phases is potentially limited in the mafic wallrocks (see previous section), the hydrothermal fluids still have ~10–50 ppm Mo in solution (Klemm et al. 2007). Based on that and considering a $D_{\mathrm{Mo}}^{\mathrm{rutile/fluid}}$ of ~1.5, the expected Mo content of rutile in equilibrium with the hydrothermal fluid would be about 15–75 ppm, significantly higher than the measured value (mean, 4.3±0.7 ppm for all alteration types; Table 2). However, contrary to felsic porphyries, most rutile in the mafic wallrocks seems to have formed simultaneously with molybdenite deposition (Fig. 8), which would explain the compositional gap (dashed area in insert Fig. 8) between rutile from the mafic wallrocks and felsic porphyries.

Although simple cooling of SO_2-rich fluids has certainly controlled sulfide precipitation (Klemm et al. 2007), the progressive decrease of temperature alone may not explain why Mo contents in rutile formed at the same temperature range (~450–550°C; Fig. 8) are more strongly buffered by MoS_2 crystallization in the mafic wallrocks than in the porphyries. Thus, an additional mechanism selectively increasing fluid $a_{(H2S)}$ has to complement simple fluid cooling in order to enhance the sulfide crystallization effect in the mafic wallrocks. Redox reactions involving S reduction during fluid mixing and/or fluid–rock interaction are a possibility. Nevertheless, isotopic evidence precludes extensive meteoric fluid participation in this deposit, even during the phyllic alteration stage (Kusakabe et al. 1984, 1990; Skewes et al. 2001). Therefore, fluid/rock interaction seems to be a more plausible means for enhanced reduction of sulfur in the mafic rocks. Since the FeO_T content is greater than five times higher in the mafic wallrocks compared to the porphyries (Table 1; Fig. 2c), strong chemical disequilibrium of fluids equilibrated with felsic rocks is to be expected during mafic wallrock alteration. The $H_2SO_{4(aq)}$ produced by progressive cooling of SO_2-rich fluids may strongly react with mafic silicates promoting additional fluid reduction and thus enhancing sulfide deposition on cooling.

Since most reactive primary minerals are probably altered throughout the early pervasive biotitization (Skewes et al. 2002), during subsequent crosscutting phyllic alteration events, an enhanced sulfide deposition in the mafic wallrocks might also be achieved through fluid reduction by interaction with the strongly biotitized wallrocks, as suggested for other deposits (e.g., Beane and Titley 1981). Therefore, redox reactions selectively operating in the mafic wallrocks may have increased $a_{(H2S)}$ in the fluids outside the felsic porphyries and enhancing MoS_2 precipitation upon fluid cooling. Under these conditions, the Mo content of the fluids may become more depleted towards mafic wallrocks and with a negligible Mo contribution from their parental phases, rutile may thus become Mo-poor. On the other hand, Mo content in rutile formed at similar temperatures (~450–550°C), but in the felsic porphyries, is higher due to the Mo-rich nature of their parental phases and the negligible effect of redox control on sulfide precipitation. In the distal propylitic zones (outside the deposit) and regardless of the nature of Ti-rich parental phases, hydrothermal rutile was equilibrated

with even cooler (≤450°C) and more Mo-depleted aqueous fluids resulting in Mo-poor rutile (3.5±0.8 ppm; Table 2).

In summary, irrespective of the alteration event considered, the marked reduction of Mo content in rutile in mafic wallrocks results from their lower temperature of formation (<550°C) compared with that in felsic rocks (mainly >550°C), coupled with a lower Mo availability due to the Mo-poor nature of Ti-rich parental phases and the MoS_2 co-crystallization on fluid cooling likely enhanced by a redox control during fluid–rock interaction owing to the sharp increase in the FeO content in the mafic wallrocks.

Sb in hydrothermal rutiles from felsic and mafic host rocks

Sulfides and rutile did not compete for Sb (Fig. 9) given the elevated solubility of the main Sb-sink phases at temperatures above 400°C (e.g., Williams-Jones and Normand 1997) where most rutile is formed. Therefore, the Sb availability in hot fluids along with a modest temperature control on Sb incorporation into the rutile structure (Fig. 9) would explain why the Sb concentration in rutile from the core to the outer fringe of the deposit remained relatively constant (Fig. 2b).

Although a priori some Sb contribution from Ti-rich phases cannot be ruled out, rutile generated from different Ti-rich parental phases (titanite + biotite vs. Fe–Ti oxides), hosted within contrasting rock types (felsic vs. mafic) and having similar Sb contents (35±3 vs. 27±4 ppm Sb; Table 2) suggests that the ore-forming fluids and not the Ti-rich parental phases may be the dominant Sb source of the hydrothermal rutile. Thus, differences between Mo and Sb regarding their temperature dependency to enter the rutile structure, their contribution from parental phases along with the differences in solubility of their dominant sulfide phases may account for the observed trend of the Mo/Sb ratio versus temperature (Fig. 5b).

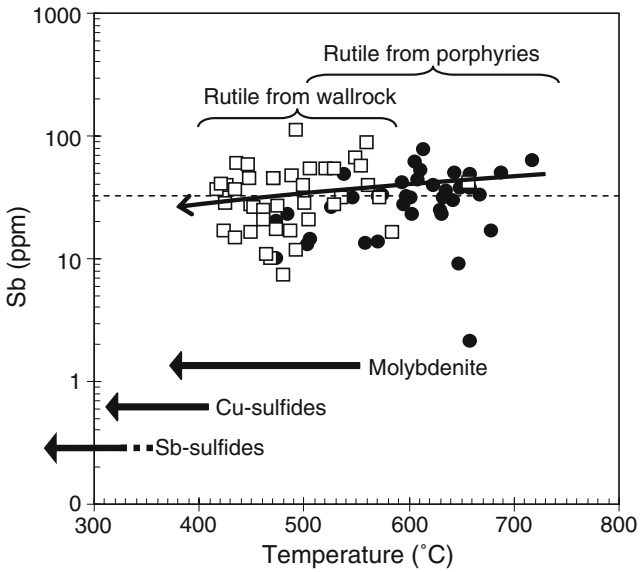

Fig. 9 Sb content versus formation temperature of rutile from the El Teniente dacite porphyry and wallrocks. Deposition temperatures of Cu-sulfides and molybdenite are from Klemm et al. 2007 and Sb-sulfides temperatures are from Williams-Jones and Normand 1997. Formation temperature of rutile calculated as in Fig. 7

Additional data and remarks

Although molybdenite deposition occurred during nearly all mineralization events (Cuadra 1986; Cannell et al. 2005), from 6.3 to 4.4 Ma (Maksaev et al. 2004), most of the reported molybdenite Re–Os ages (Maksaev et al. 2004; Cannell et al. 2005) cluster around ~5.0 and 4.7 Ma. Since the Re–Os system in MoS_2 does not appear to have been disturbed by successive hydrothermal overprinting (Maksaev et al. 2004) and considering that samples with that range of ages are distributed throughout the deposit, it is hard to avoid the conclusion that an important input of Mo-bearing fluids into the plumbing system of the deposit took place during the latest stage of dacite magma activity. Sample TT-91 used by Maksaev et al. (2004) for dating latite ring dikes, which surround the Braden breccia pipe and are the shallow expression of this late dacite activity, was used for additional PIXE analyses on rutile (see full petrographic description of this sample in Maksaev et al. 2004).

Despite of the chemical similarity between all dacite porphyries from El Teniente, (e.g., Table 1, Skewes et al. 2002; Table 4, Cannell et al. 2005; Table 5, González 2006), rutile from the latite dikes is not enriched in Mo (6–7 ppm; n=2). The temperature of formation calculated for these rutile samples (~550°C) does not favor a scenario of co-crystallization with MoS_2, since most MoS_2 precipitated at <550°C (Fig. 6f, Klemm et al. 2007). Besides, Mo contents in rutile from the El Teniente dacite porphyry, formed at the same temperature than that of the ring dikes, are one order of magnitude higher (60-70 ppm Mo; Fig. 8), suggesting that the main limiting factor preventing Mo enrichment in these rutile samples may likely be related to Mo availability.

Given the close compositional and mineralogical affinity of all dacite rocks of the El Teniente deposit, it is speculated that early volatile saturation of the felsic melt feeding the latite dikes could account for the Mo-poor nature of these rutile crystals. Owing to the strong partitioning of Mo into the ore-forming aqueous phase during melt-fluid separation (Candela and Holland 1984), early fluid exsolution would efficiently deplete the melt in Mo limiting its incorporation into the crystallizing Ti-rich

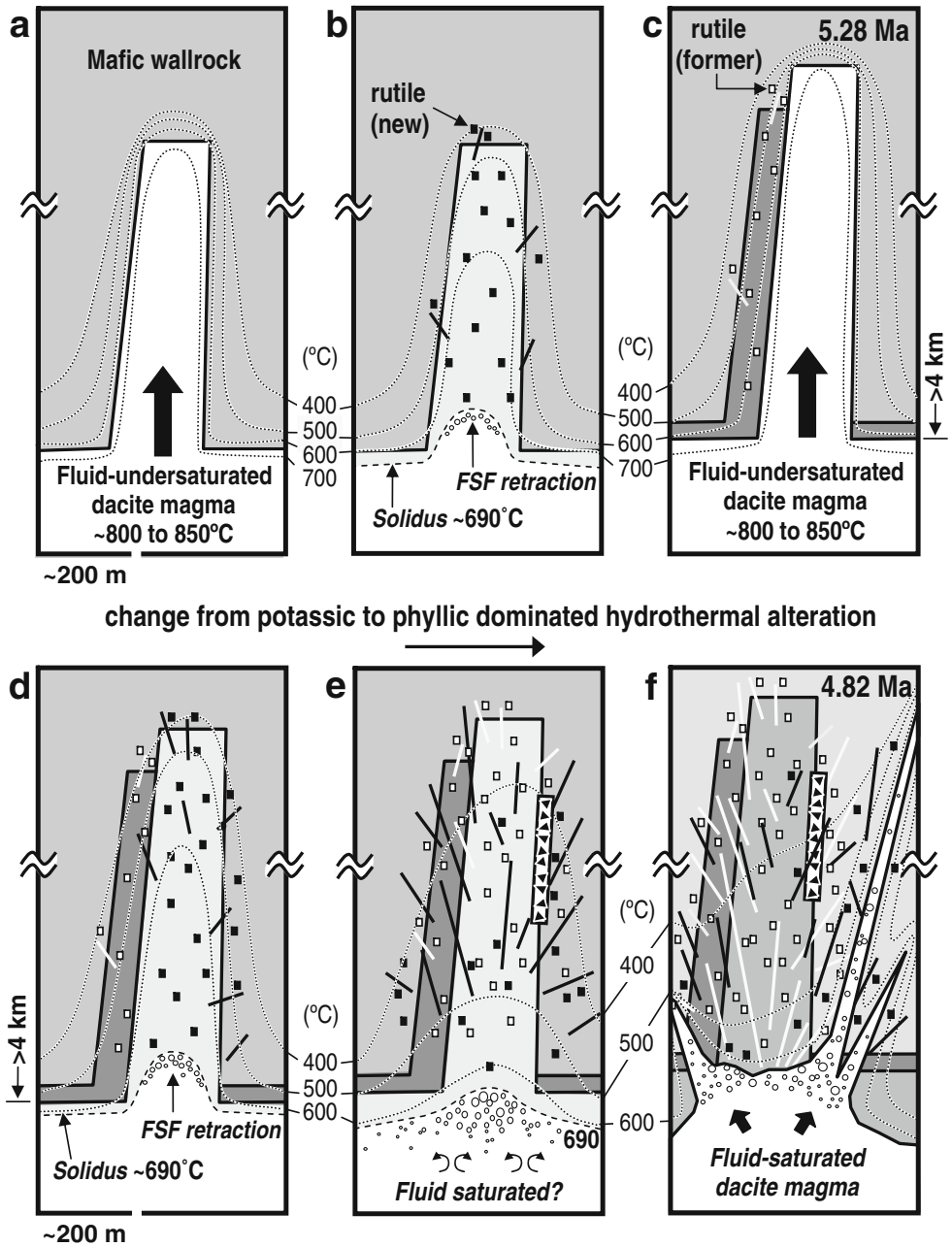

Fig. 10 Schematic cross section (~600 N) of the El Teniente dacite porphyry summarizing the multistage formation of rutile. Depth of the underlying magma reservoir (≥4 km) inferred from amphibole stability (≥1 kbar). Magmatic temperatures were estimated after Scaillet and Evans 1999. Isotherms were visually estimated. **a** Early phase intrusion of the El Teniente dacite porphyry. **b** The thin (≤200 m wide for the top 800 m; Rojas 2002), steep-walled, tabular geometry favors large a lateral thermal gradient inducing initially rapid sidewall crystallization. A short-lived magmatic activity may be envisaged, at least for the apical portion of this intrusion. Volatile exsolution at the emplacement level may have initially been induced by decompression, followed by crystallization-driven exsolution at the down-migrating fluid saturation front (*FSF*), until the intrusion solidifies. Exsolved volatiles altered the already solidified rim of the dacite porphyry and nearby wallrocks, forming hydrothermal rutile after Ti-rich accessory phases. **c** and **d** Due to its similarity in shape, size, level of emplacement, and composition the next intrusive pulse (5.28 Ma) evolved analogously to the former. **e** The FSF propagates down to deeper levels with progressive cooling of the intrusion. Fluids fluxed upward through the porphyry and along structures generated additional rutile linked to phyllic-dominated alteration. **f** Continuous degassing of the underlying saturated dacite magma remained undisturbed until 4.82 Ma, when late dacite plugs and ring dikes were intruded and the whole system was depressurized by the formation of the Braden breccia pipe. Early fluid saturation may have led to the formation of Mo-poor rutile in these late porphyries (see text). Hydrothermal activity lasted until at least 4.37 Ma

accessory phases from which rutile is derived. The widespread MoS_2 mineralization associated with the later dacite magmas, as well as its explosive nature represented by the Braden diatreme, may in part be a consequence of an early volatile-rich state.

Figure 10 schematically summarizes the multistage formation of rutile in connection with the magmatic–hydrothermal evolution of the El Teniente system (the older apophyses and dacite pipes are omitted for simplicity).

Conclusions

Most hydrothermal rutile in the El Teniente porphyry Cu–Mo deposit nucleated and grew at the original textural position (e.g., rutile pseudomorphs, sagenitic texture) of its igneous Ti-rich parent mineral phase. Rutile formed by re-equilibration and/or breakdown of titanite, biotite, Ti-magnetite, and ilmenite within a relatively broad temperature range (~400 to 700°C) and under fluid-dominated conditions.

Despite the giant nature and protracted history of mineralization of the El Teniente deposit, the Mo content of rutile broadly changes with its position in the orebody. High-temperature (~500–700°C), Mo-rich rutile (186±20 ppm) dominates in felsic porphyries while lower-temperature (~400–550°C), Mo-poor rutile (5.4±1.1 ppm) dominates in the mafic wallrocks. In addition to temperature, Mo content of rutile also depends on Mo availability, i.e., Mo content of the hydrothermal fluid system and Mo/Ti ratio of Ti-rich parental phases, both of which are controlled by melt composition, fO_2 and timing of fluid–melt separation. The modal abundance and stability under varying hydrothermal conditions of the Ti-rich parental mineral phases are also important in defining rutile chemistry.

In felsic porphyries, the high-temperature (>550°C), oxidized and low $a_{(H2S)}$ hydrothermal fluids delayed or suppressed sulfide precipitation to temperatures below ~550°C, enhancing Mo partitioning into high-temperature rutile (Mo-rich rutile in low-grade ore zones). Under these hydrothermal conditions, most Mo scavenged from the dacite melt by early crystallizing (i.e., prior to volatile exsolution) Ti-rich mineral phases is transferred into residual rutile preventing its partitioning into the fluid phase. Therefore, the timing of volatile phase separation in the felsic magmas places a constraint on fluid and rutile chemistry. We suggest that the low Mo content of rutile from late latite dikes may be a result of early fluid phase exsolution of the magma source feeding these dikes, leading to Mo-depleted Ti-rich parent mineral phases.

With fluid temperature decreasing below ~550°C molybdenite becomes stable and Mo starts to partition into the sulfide phase (chalcophile affinity). As a result, rutile becomes Mo-poor, particularly in the colder, FeO-rich mafic wallrocks where Mo derived from Ti-rich parental phases is limited and sulfide precipitation more efficient (high-grade ore zone). The control on sulfide deposition exerted by mafic wallrocks was likely twofold: (1) simple cooling, and (2) $SO_{2(aq)}$ reduction through fluid–rock interaction enhancing MoS_2 deposition. Thus, at lower temperatures (≤550°C) sulfide precipitation and the efficiency of this process also place a constraint on rutile chemistry. The combination of the aforementioned variables allows to explain the abrupt change in Mo content of rutile across the porphyry-mafic-wallrock contacts.

The high solubility of Sb at temperatures above ~400°C, in conjunction with the poor temperature dependency of Sb entering the rutile structure explains the relatively constant Sb contents in hydrothermal rutile from all parts of the deposit (35±3 ppm Sb).

The origin and compositional changes of hydrothermal rutile presented here, along with the age and nature of the dacite magmas, are compatible with the model in which the felsic porphyries and associated structures were fluxed by hot (>550°C), oxidized (fO_2 ≥NNO +1.3), SO_2-rich, Mo (and Cu)-bearing ore-forming fluids. These fluids were likely exsolved from the small crystallizing porphyries and their underlying much larger magmatic reservoirs resulting in a comparatively low-grade ore zone in the hot and oxidized felsic intrusives as opposed to the cooler, reduced and more reactive mafic wallrocks, where high-grade ore was deposited upon fluid cooling.

Acknowledgments Earlier versions of this manuscript benefited from thoughtful comments by J. Richards, J. Otamendi, and helpful discussions with C. Heinrich. We thank B. Townley and D. Cooke for critical reviews, and B. Lehmann for careful editorial handling. We also gratefully acknowledge the El Teniente Division of CODELCO for logistic support during this study. Special thanks to T.T. Win and W. Przybyłowicz for PIXE analyses and to V. Maksaev for kindly providing a ring dike sample for additional PIXE analyses. Chilean FONDECYT #198-0511 and FONDECYT Líneas Complementarias #800-0006 financed this research.

References

Ayers JC, Watson EB (1993) Rutile solubility and mobility in supercritical aqueous fluids. Contrib Mineral Petrol 114:321–330

Beane RE, Titley SR (1981) Porphyry copper deposits. Part II. Econ Geol 75:214–269

Blount CW, Dickinson FW (1969) The solubility of anhydrite ($CaSO_4$) in NaCl–H_2O from 100 to 450°C and 1 to 1,000 bars. Geochem Cosmochim Acta 33:227–245

Camus F (1975) Geology of El Teniente orebody with emphasis on wall-rock alternation. Econ Geol 70:1341–1372

Candela PA (1997) A review of shallow, ore-related granites: textures, volatiles and ore metals. J Petrol 38:1619–1633

Candela PA, Bouton SL (1990) The influence of oxygen fugacity on tungsten and molybdenum partitioning between silicate melt and ilmenite. Econ Geol 85:633–640

Candela PA, Holland HD (1984) The partitioning of copper and molybdenum between silicate melts and aqueous fluids. Geochim Cosmochim Acta 48:373–380

Cannell J, Cooke DR, Stein HJ, Markey R (2003) New paragenetically constrained Re-Os molybdenite ages for El Teniente Cu-Mo porphyry deposit, central Chile. In: Eliopoulos et al (eds) Mineral exploration and sustainable development. Millpress, Rotterdam, pp 255–258

Cannell J, Cooke D, Walshe J, Stein H (2005) Geology, mineralization, alteration, and structural evolution of the El Teniente porphyry Cu–Mo deposit. Econ Geol 100:979–1003

Cannell J, Cooke D, Walshe J, Stein H (2007) Geology, mineralization, alteration and structural evolution of El Teniente porphyry Cu–Mo deposit—a reply. Econ Geol 102:1171–1180

Cao X (1989) Solubility of molybdenite and the speciation of molybdenum in hydrothermal solutions: Unpublished PhD thesis, Ames, Iowa State University, 102 p

Carroll MR, Rutherford MJ (1985) Sulfide and sulfate saturation in hydrous magmas. Proc 15th Lunar Plan Sci Conf. J Geophys Res 90:C601–612

Carroll MR, Webster JD (1994) Sulfur, noble gases, and halogens: solubility relations of the less abundant volatile species in magmas. In Carroll MR, Holloway JR (eds). Rev Mineral 30:331-371

Chambefort I, Dilles JH, Kent AJR (2008) Anhydrite-bearing andesite and dacite as a source for sulfur in magmatic–hydrothermal mineral deposits. Geology 36:719–722

Cuadra P (1986) Geocronología K–Ar del yacimiento El Teniente y áreas adyacentes. Rev Geol Chile 27:3–26

Czamanske GK, Force ER, Moore WJ (1981) Some geologic and potential resources aspects of rutile in porphyry copper deposits. Econ Geol 76:2240–2245

Fitton JG (1995) Coupled molybdenum and niobium depletion in continental basalts. Earth Planet Sci Lett 136:715–721

Force ER (1991) Geology of titanium-mineral deposits. GSA, Special Paper 259, 112 p

Ghiorso MS, Sack RO (1991) Thermochemistry of the oxide minerals. In: DH Lindsley (ed) Oxide Minerals: Petrologic and Magnetic Significance, Mineralogical Society of America Reviews in Mineralogy 25:221-264

González RA (2006) Petrografía, geoquímica y microtermometría de los intrusivos félsicos del sector norte del yacimiento El Teniente. Memoria de Título, Univer. de Concepción, 149 p

Gunow AJ (1983) Trace element mineralogy in the porphyry molybdenum environment. PhD Tesis, University of Colorado, 304 p

Guzmán C (1991) Alteración y mineralización de los pórfidos dioríticos del sector central, yacimiento El Teniente, Unpubl BSc thesis, Santiago, Universidad de Chile, 145 p

Haggerty SE (1991) Oxide textures—a mini atlas. In: Lindsley DH (ed) Oxide minerals: petrologic and magnetic significance. Rev Mineral 25:129-219

Hattori KH, Guillot S (2003) Volcanic fronts form as a consequence of serpentinite dehydration in the forearc mantle wedge. Geology 31:525–528

Hernández LB, Rabbia OM, King RW, López-Escobar L (2002) Sulfur-rich apatite from intrusive rocks associated with the supergiant El Teniente porphyry Cu-Mo deposit, Chile. 18th General Meeting of the Int Miner Assoc, Mineralogy for the Millennium, Progr with abstracts, Edinburgh, Scotland, p 268

Hernández LB, Rabbia OM, King RW, Lopéz Escobar L (2004) Metasomatic monazite in apatites from felsic porphyries related to Cu-Mo mineralization. Abstract, Goldschmidt Conference, Geochim Cosmochim Acta 68: A309

Howell FH, Molloy JS (1960) Geology of the Braden orebody, Chile, South America. Econ Geol 55:863–905

Kay SM, Mpodozis C, Coira B (1999) Neogene magmatism, tectonism and mineral deposits of the Central Andes (22º-33ºS). In Skinner BJ (ed), Geology and ore deposits of the Central Andes. Soc Econom Geol, Spec Publ 7:27-59

Keith JD, Whitney JA, Hattori K, Ballantyne GH, Christiansen EH, Barr DL, Cannan TM, Hook CJ (1997) The role of magmatic sulfides and mafic alkaline magmas in the Bingham and Tintic Mining Districts, Utah. J Petrol 38:1679–1690

Keppler H, Wyllie PJ (1991) Partitioning of Cu, Sn, Mo, W, U, and Th between melt and aqueous fluid in the systems haplogranite–H_2O–HCl and haplogranite–H_2O–HF. Contrib Mineral Petrol 109:139–150

Klemm LM, Pettke T, Heinrich CA, Campos E (2007) Hydrothermal evolution of the El Teniente deposit (Chile): porphyry Cu-Mo ore deposition from low-salinity magmatic fluids. Econ Geol 102:1021–1045

Kusakabe M, Nakagawa S, Hori M, Matsuhisa Y, Ojeda JM, Serrano L (1984) Oxygen and sulfur isotopic compositions of quartz, anhydrite and sulfide minerals from the El Teniente and Río Blanco porphyry copper deposits, Chile. Bull Geol Surv Japan 35:583–614

Kusakabe M, Nakagawa S, Hori M, Matsuhisa Y (1990) Primary mineralization-alteration of the El Teniente and Río Blanco porphyry copper deposits, Chile: stable isotope, fluid inclusion and $Mg^{+2}/Fe^{+2}/Fe^{+3}$ ratios of hydrothermal fluids. In: Herbert HK, Ho SE (eds) Stable isotopes and fluid processes in mineralization. Univ. of Western Australia Press, Perth, pp 244–259

Larocque ACL, Stimac JA, Keith JD, Huminicki MAE (2000) Evidence for open-system behavior in immiscible Fe–S–O liquids in silicate magmas: implications for contributions of metals and sulfur to ore-forming fluids. Can Mineral 38:1233–1249

Lowell JD, Guilbert JM (1970) Lateral and vertical alteration–mineralization zoning in porphyry copper deposits. Econ Geol 65:373–408

Luhr JF, Carmichael ISE, Varekamp JC (1984) The 1982 eruptions of El Chichón Volcano, Chiapas, Mexico: mineralogy and petrology of the anhydrite-bearing pumices. J Volcan Geoth Res 23:69–108

Maksaev V, Munizaga F, McWilliams M, Fanning M, Mathur R, Ruiz J, Thiele K (2002) El Teniente porphyry copper deposit in the Chilean Andes: new geochronological timeframe and duration of hydrothermal activity. GSA Meeting 2002, Abstract, 34:336

Maksaev V, Munizaga F, McWilliams M, Fanning M, Mathur R, Ruiz J, Zentilli M (2004) New chronology for the El Teniente, Chilean Andes, from U-Pb, $^{40}Ar/^{39}Ar$, Re-Os, and fission-track dating: implications for the evolution of a supergiant porphyry Cu-Mo deposit. Econ Geol Spec Publ 11:15–54

Mason B (1966) Principles of geochemistry, 3rd edn. Wiley, p 329

Munizaga F, Maksaev V, Mathur R, Ruiz J, McWilliams M, Thiele K (2002) Understanding molybdenite Re-Os ages from the El Teniente porphyry copper deposit, Chile. GSA Meeting Abstr with Progr 34:336

Nash WP, Crecraft HR (1985) Partition coefficients for trace elements in silicic magmas. Geochim Cosmochim Acta 49:2309–2322

Ojeda JM, Hernández E, Ossandón G, Enrione A, Mestre A (1980) El Pórfido cuprífero El Teniente. CODELCO, Chile, p 72 IR, Superintendencia de geología de El Teniente

O'Neill HSC, Eggins SM (2002) The effect of melt composition on trace element partitioning: an experimental investigation of the activity coefficients of FeO, NiO, CoO, MoO_2 and MoO_3 in silicate melts. Chem Geol 186:151–181

Ossandón G (1974) Petrografía y alteración del pórfido dacítico, yacimiento El Teniente. Universidad de Chile, Memoria de Título, 116 p

Piccoli P, Candela P, Rivers M (2000) Interpreting magmatic processes from accessory phases: titanite—a small-scale recorder of large-scale processes. Transact R Soc Edingburgh: Earth Sci 9:257–257

Rabbia OM (2002) Cristaloquímica de rutilo y anatasa en sistemas de pórfidos cupríferos andinos: evaluación de su uso como monitores de la actividad de metales en fluidos hidrotermales corticales. Unpublished PhD thesis, Universidad de Chile, 147 p

Rabbia OM, Reich M, Hernández LB, King RW, López-Escobar L (2000) High-Al TTG-like suite at the El Teniente porphyry copper deposit, Chile. Ext Abstr, IX Congr Geol Chileno, July 31- August 4, Puerto Varas, Chile. 5:326–329

Rabbia OM, Hernández LB, King RW, López-Escobar L (2001) Sr-Nd-Pb isotope compositions of felsic intrusions in the El Teniente and Laguna La Huifa areas, central Chile. Ext Abstr, III South American Symposium on Isotope Geology, 10/21-24th, Pucón, Chile. CD format

Rabbia OM, Hernández LB, Townley B, King RW, Ayers JC (2003) Anatase-bearing veins in the El Teniente Cu-Mo porphyry system. Special Symposium on Supergiant Andean Porphyry Copper Deposits. 10°Cong Geol Chileno. October 6-10, Concepción, Chile, CD-format

Reich MH (2001) Estudio petrográfico, mineraloquímico y geoquímico de los cuerpos intrusivos de Sewell y La Huifa, Yacimiento El Teniente, VI Región, Chile. Memoria de Título, Universidad de Concepción, 111 p

Ribbe PH (1982) Titanite. In: Ribbe PH (ed) Orthosilicates. Rev Mineral 5:37-155

Rojas A (2002) Petrografía y geoquímica del pórfido Teniente, ubicado en el sector norte del yacimiento El Teniente, Provincia de Cachapoal, VI Region, Chile, Memoria de Título, Universidad de Concepción, 133 p

Ryan CG, Cousens DR, Sie SH, Griffin WL, Suter GF, Clayton E (1990) Quantitative PIXE microanalysis of geological material using the CSIRO proton microprobe. Nucl Instr Meth B47:55–71

Scaillet B, Evans BW (1999) The 15 June 1991 eruption of Mount Pinatubo. I. Phase equilibria and pre-eruption P–T–fO_2–fH_2O conditions of the dacitic magma. J Petrol 40:381–411

Scaillet B, Clemente B, Evans BW, Pichavant M (1998) Redox control of sulfur degassing in silicic magmas. J Geophys Res 103:B10:23,937-23,949

Skewes A (2000) Rocas ígneas de la mina El Teniente. CODELCO Internal report 94 p

Skewes MA, Arévalo AG (2000) El complejo de gabros y diabasas que hospeda a las brechas mineralizadas del depósito de cobre El Teniente. Chile central, IX Cong Geol Chileno, Puerto Varas 1:380–384

Skewes A, Stern CR (2007) Geology, mineralization, alteration and structural evolution of El Teniente porphyry Cu-Mo deposit—discussion: Econ Geol 102:1165-1170

Skewes A, Arevalo A, Holmgren C, Stern CR (2001) Stable isotope evidence for the formation from magmatic fluids of the mineralized breccias in the Los Bronces and El Teniente copper deposits, Central Chile: III Simposio Sudamericano de Geología Isotópica, Pucón, Chile, Extended abstracts, CD-ROM, pp 531-534

Skewes A, Arevalo A, Floody R, Zuñiga P, Stern CR (2002) The El Teniente Breccia deposit: hypogene copper distribution and emplacement. Soc Econ Geol, Spec Publ 9:299–332

Skewes A, Arevalo A, Floody R, Zuñiga P, Stern CR (2005) The El Teniente megabreccia deposit, The world's largest deposit. In Poter TM (ed) Super porphyry copper and gold deposits- a global perspective: Porter Geoscience Consultancy Publishing, Adelaide, Australia. 1:83-113

Sillitoe RH, Perelló J (2005) Andean copper province: tectonomagmatic settings, deposits types, metallogeny, exploration, and discovery. In Hedenquist JW, Thompson JFH, Goldfarb RJ, Richards JP (eds) Econ Geol One Hundredth Anniversary Volume:845-891

Stimac J, Hickmott D (1994) Trace-element partition-coefficients for ilmenite, ortho-pyroxene and pyrrhotite in rhyolite determined by micro-pixe analysis. Chem Geol 117:313–330

Tacker RC, Candela PA (1987) Partitioning of molybdenum between magnetite and melt. A preliminary experimental study of partitioning of ore metals between silicic magmas and crystalline phases. Econ Geol 82:1827–1838

Tomkins HS, Powell R, Ellis DJ (2007) The pressure dependence of the zirconium-in-rutile thermometer. J Metam Geol 25:703–713

Udubasa G (1982) Rutile of post-magmatic mineral formation. In: GC Amstutz (ed) Ore genesis - the state of the art. Berlin, Springer, 784-793

Ulrich T, Mavrogenes J (2008) An experimental study of the solubility of molybdenum in H_2O and KCl–H_2O solutions from 500 to 800°C, and 150 to 300 MPa. Geochim Cosmochim Acta 72:2316–2330

Williams S, Cesbron F (1977) Rutile and apatites: useful prospecting guides for porphyry copper deposits. Mineral Mag 41:288–292

Williams-Jones AE, Normand C (1997) Controls of mineral paragenesis in the system Fe–Sb–S–O. Econ Geol 92:308–324

Zack T, Kronz A, Foley SF, Rivers T (2002) Trace element abundances in rutiles from eclogites and associated garnet mica schists. Chem Geol 184:97–122